American Mineralogist, Volume 84, pages 1319–1332, 1999

Experimental determination of CO_2-H_2O activity-composition relations at 600–1000 °C and 6–14 kbar by reversed decarbonation and dehydration reactions

L.Y. ARANOVICH AND R.C. NEWTON*

Department of the Geophysical Sciences, University of Chicago, 5734 S. Ellis Avenue, Chicago, Illinois 60637, U.S.A.

ABSTRACT

Activity-composition relations in CO_2-H_2O solutions were determined at 6, 10, and 14 kbar over broad temperature-fluid composition ranges from 70 reversed determinations of three simple-system decarbonation and dehydration reactions:

$CaCO_3 + SiO_2 = CaSiO_3 + CO_2$ (WQC)
calcite quartz wollastonite

$MgCO_3 + MgSiO_3 = Mg_2SiO_4 + CO_2$ (FEM)
magnesite enstatite forsterite

$Mg_3Si_4O_{10}(OH)_2 = 3\ MgSiO_3 + SiO_2 + H_2O$ (TEQ)
talc enstatite quartz

Brackets of WQC and FEM were achieved by reversing, at constant T and P, the fluid composition coexisting with the assemblages of either reaction, starting with fine-grained mixtures of reactants and products in nearly equimolar amounts and liquid water, oxalic acid, and silver oxalate as fluid sources. Brackets of TEQ were secured by reversing the reaction over narrow temperature intervals at constant P and fluid composition. All experiments were made in the piston-cylinder apparatus with NaCl or NaCl-soft glass pressure media, and all experiments with two-component fluids were buffered at hematite-magnetite. Closure intervals of reversed fluid composition averaged less than 2 mol% CO_2. Activity values of H_2O (1) and CO_2 (2) were retrieved based on the THERMOCALC 2.3 thermodynamic data set of Holland and Powell (1994), which includes equations of state of H_2O and CO_2, supplemented by several tight reversals of the end-member equilibria. A simple van Laar-type expression reproduces our composition determinations with a standard deviation of only 1.2 mol% CO_2:

$$RT \ln\gamma_1 = (X_2)^2 W\{V_1^0 V_2^{0^2}/[(V_1^0+V_2^0)(X_1V_1^0+X_2V_2^0)^2]\}$$

$$RT \ln\gamma_2 = (X_1)^2 W\{V_2^0 V_1^{0^2}/[(V_1^0+V_2^0)(X_1V_1^0+X_2V_2^0)^2]\}$$

where V_1^0 and V_2^0 are, respectively, the specific volumes of pure H_2O and CO_2 at a given (P,T), the X's are the mole fractions, the γ's the activity coefficients and W is analogous to a regular solution parameter: $W = (A+BT)[1-\exp(-20P)] + CPT$, with T in K and P in kbar. The best-fit values of the constants are: A = 12893 J, B = –6.501 J/K, C = 1.0112 J/(K·kbar). With these formulas, the activity-concentration relations of CO_2-H_2O solutions may be reconstructed in a broad P-T-X range using any reasonably accurate equations of state of pure CO_2 and H_2O. The activity-concentration relations are closely similar to the modified Redlich-Kwong (MRK) reconstruction of Kerrick and Jacobs (1981) to pressures of 6 kbar, but the binary fluids have marginally greater positive non-ideality than the MRK predictions at 10 kbar and significantly greater non-ideality at 14 kbar. The present results can serve as a basis for reliable calculations of mineral-fluid equilibria in metamorphism of the deep crust and upper mantle.

INTRODUCTION AND PREVIOUS WORK

Water and carbon dioxide are the two most abundant volatile species in the outer parts of the Earth; their mixtures form the common solvents in which varying amounts of solutes, principally subordinate volatiles and soluble salts, make up complex natural fluids. Thermodynamic properties of the binary join CO_2-H_2O are therefore fundamental controls on the behavior of natural fluids in the outer parts of the Earth's interior.

Precise experimental measurements of the specific volume of CO_2 to 700 °C and 8 kbar were made by Shmonov and Shmulovich (1974) in a gas-pressure vessel. These data were extrapolated to 10 kbar and 1000 °C in the widely used tables of Shmulovich and Shmonov (1978), which present fugacity (f^0) data derived from the volume (V^0) measurements. The fugacity, which is defined by the relationship (where R is the gas constant):

$$RT \ln f^0 = \int_{1\text{bar}}^{P} V^0 dP = G(T,P) - G(T,1) \qquad (1)$$

*E-mail: rcnewton@midway.uchicago.edu

0003-004X/99/0009–1319$05.00

measures the Gibbs free energy (G) of compression, and is therefore of great practical utility in calculation of chemical equilibrium in volatile-bearing systems.

Interpolation and extrapolation of the CO_2 thermodynamic properties have been made with the use of various theoretical equations of state (EOS). The most widely used of these is the Redlich-Kwong equation, first used for calculations of mineralogical equilibria by Holloway (1977). His modified Redlich-Kwong (MRK) equation is:

$$P = RT/(V-\mathbf{b}) - \mathbf{a}/[V(V+\mathbf{b})\sqrt{T}] \qquad (2)$$

The parameter **a** was considered to be a function of temperature only, and **b** to be independent of both temperature and pressure. The mathematical simplicity of the MRK equation and its ability to model measured P-V-T data for CO_2 and H_2O in the low-pressure region have encouraged much subsequent use and recalibration (Kerrick and Jacobs 1981; Bottinga and Richet 1981; Halbach and Chatterjee 1982; Holland and Powell 1991). The **b** parameter is closely analogous to the excluded volume parameter of the simple van der Waals equation, where compression is considered to affect the distances between molecules, but not the sizes of molecules themselves. This "hard-sphere" aspect of the theory tends to result in overestimation of the fluid volumes and fugacities at very high pressures. Haselton et al. (1978) determined the P-T curves of several decarbonation reactions involving magnesite and calcite at pressures up to 40 kbar and temperatures to 1500 °C in a piston-cylinder solid-pressure device. They concluded from their data that the MRK equation of Holloway (1977) overestimated CO_2 fugacities by as much as a factor of two in the highest P-T range. A more compressible fluid is provided by allowing **b** to be a function of pressure, as was done by Halbach and Chatterjee (1982), but the formulations become much more difficult mathematically. As a compromise, Holland and Powell (1991) added a compensating term to the volume that satisfies Equation 2, V(MRK):

$$V = V(\text{MRK}) + \mathbf{c}\sqrt{(P-P^0)} + \mathbf{d}(P-P^0) \qquad (3)$$

where **c** and **d** are functions of T only, and P^0 is a representative pressure, different for each gas, where the simple MRK equation begins to overestimate the volume. The additional terms yield a negative contribution to the volume that increases with pressure. This model yields better agreement of CO_2 fugacity with the high-pressure decarbonation data as well as a close fit to the lower pressure P-V-T measurements.

Alternative formulations are based more directly on experimental high P-T phase equilibria. Mäder and Berman (1991) constrained CO_2 volumes and fugacities above 10 kbar to satisfy experimental data on decarbonation reactions. The most important and well-studied of these reactions are:

(A) $CaCO_3 + SiO_2 = CaSiO_3 + CO_2$ (WQC)
calcite quartz wollastonite

(B) $MgCO_3 + MgSiO_3 = Mg_2SiO_4 + CO_2$ (FEM).
magnesite enstatite forsterite

Use of the WQC reaction in the higher temperature range is subject to the uncertainty surrounding the disordering transition in calcite above 1000 °C (Redfern et al. 1989), which has not been fully accounted for in its possible effects on the dP/dT slope of WQC. Holland and Powell (1994) treated the transition as higher order, with heat capacity incremented by a Landau-type term as the critical temperature is approached. The rapid increase in the volume of calcite as the critical temperature is approached, shown by the neutron diffraction measurements of Dove and Powell (1989), is not specifically addressed in the THERMOCALC 2.3 program of Holland and Powell (1994). The transition was treated as first-order by Mäder and Berman (1991) in both thermal and volumetric aspects (see Fig. 1). Data available to define the FEM curve in the pressure range below 15 kbar have not been available before the recent study of Koziol and Newton (1998). The unreversed determinations of Newton and Sharp (1975) at higher pressures, used by Mäder and Berman (1991), are limited in their application by uncertainties in magnesite volume at very high temperatures and pressures. The Mäder and Berman (1991) formulation has the

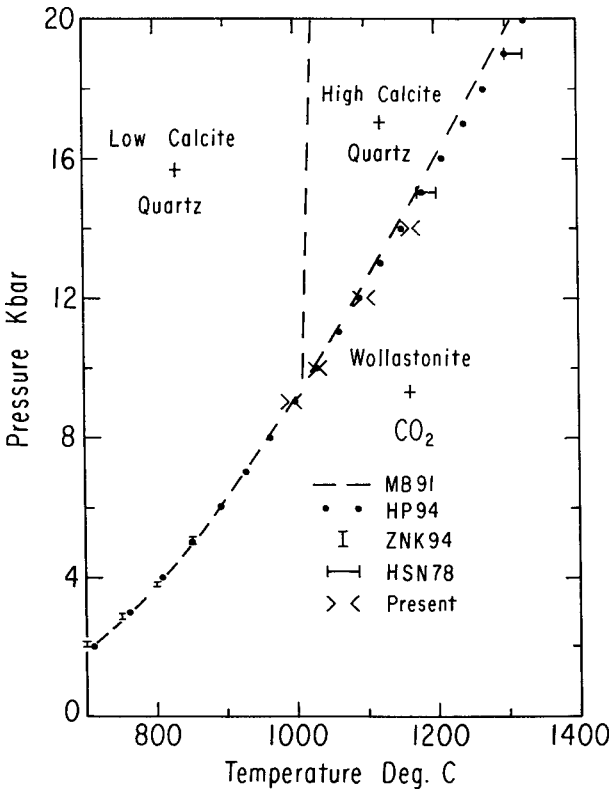

FIGURE 1. Experimental and calculated data on the WQC reaction (Equation A, text). Reversed brackets include four of Zhu et al. (1994) at lower pressures (ZNK 94), and four brackets of the present study. Also shown are the unreversed brackets of Haselton et al. (1978) from observation of decarbonation or lack of decarbonation in calcite-quartz mixtures in unsealed platinum capsules in the piston-cylinder apparatus with soft glass pressure medium. The curves predicted by the self-consistent data sets of Mäder and Berman (1991) and THERMOCALC 2.3 (HP 94) from the paper of Holland and Powell (1994) are shown. All of the data are in excellent agreement to temperatures of at least 1020 °C, at the calcite disordering transition. The high-low calcite phase boundary is from Mäder and Berman (1991). The present CO_2 activities are modeled on low calcite, using the Holland and Powell (1994) data set.

disadvantage that their CO_2 equation of state is tied to a set of simultaneously derived thermodynamic properties of calcite and magnesite that have not been measured independently. Frost and Wood (1995; 1997a) experimentally determined the equilibrium oxygen fugacity of the graphite/diamond-O_2-CO_2 reaction to 77 kbar and 1650 °C in piston-cylinder and multi-anvil devices and derived corresponding CO_2 fugacities. These reconstructions yield lower fugacities at pressures above 10 kbar than the purely MRK-based equations.

Volumes and fugacities of H_2O have been determined in many experimental studies, the most comprehensive of which is that of Burnham et al. (1969) in a gas-pressure vessel. EOS based on virial formulas (e.g., Haar et al. 1984) give a good account of the *P-V-T* data, all of which were taken below 8 kbar, but have been shown on the basis of experimental dehydration equilibria to be deficient models for the extrapolation of the properties of H_2O above 10 kbar (Pawley and Wood 1994). EOS that are more successful are those constrained in the very high pressure range by shock-wave data (Sharp 1962; Halbach and Chatterjee 1982; Bulakh 1979). The compensated Redlich-Kwong (CORK) EOS of Holland and Powell (1991) yields volumes and fugacities of H_2O up to 50 kbar and 1500 °C that are in fairly close agreement with the experiments.

Experimental determination of thermodynamic properties of CO_2-H_2O mixtures is more difficult than for the pure gases, and the database is quite limited. The most important quantity to be derived is the relative fugacity, or activity, of a component, a_i, defined by:

$$a_i = f_i/f_i^0 = \gamma_i X_i \tag{4}$$

where f_i is the fugacity of the component in the mixture, f_i^0 is the fugacity of the pure component i at the same *P-T* conditions, X_i is the mole fraction of the component, and γ_i is the activity coefficient of component i. Fugacity and activity are related to the partial molar volumes of the components in the mixture by relationships similar to Equation 1:

$$RT \ln f_i = RT \ln X_i + \int_1^P V_i dP_{T,xi=Const} \tag{5}$$

$$RT \ln a_i = RT \ln X_i + \int_1^P \left(V_i - V_i^0\right) dP_{T,xi=Const} \tag{6}$$

where V_i is the partial molar volume of component i. These equations assume ideal behavior of the components at one bar.

Reviews of the experimental work on mixing properties in the H_2O-CO_2 binary are given by Shmulovich (1988), Duan et al. (1992), and Anovitz et al. (1998). The earlier experimental studies measured volumes of mixtures as functions of *T*, *P*, and composition in gas-pressure vessels, and have covered rather limited ranges of pressure and temperature (see Table 3 in Duan et al. 1992). The low-pressure data (up to 500 bars at 450–800 °C: Greenwood 1969, 1973) show nearly ideal volume and activity behavior ($a = x$) at the highest temperatures, but progressively positive ($a > x$) deviations from ideality at lower temperatures. The deviations are asymmetric, with largest activity coefficients in the dilute ranges of both components. Seitz and Blencoe (1996) reported precise density measurements on CO_2-H_2O mixtures with a vibrating densimeter. They found large deviations from ideal volume behavior at 400 °C and 1000 bars. Synthetic fluid inclusion techniques have provided limited volumetric data in the *P-T* range to 700 °C and 6 kbar (Sterner and Bodnar 1991) and, most recently, to 1400 °C and 19 kbar (Frost and Wood 1997b). The latter experiments, on synthetic fluid inclusions in corundum, have clearly demonstrated that the mixtures retain significant positive excess volume at high pressures even at 1400 °C. Although some of the volumetric measurements are very precise, differentiation with respect to composition (to obtain partial quantities) and integration over a large pressure range may accrue large uncertainties in the calculated activities. Moreover, standard volumes of pure end-member gases, V_i^0, which are directly involved in the activity calculations from the volumetric measurements (Eq. 6), usually are not determined in the same set of experiments, and this may lead to strongly different estimates of the excess volumes.

Less-direct measurements of H_2O activity are provided by the hydrogen sensor (Chou and Williams 1979) and hydrogen membrane (Joyce and Holloway 1993; Anovitz et al. 1998) techniques. The most recent study with the latter technique (Anovitz et al. 1998) has found positive deviations from ideality at 500 °C and 0.5 kbar significantly greater than those predicted by the volumetric measurements.

Greenwood (1967) was the first to estimate CO_2 activity in H_2O mixtures with the displaced equilibrium method. At fixed pressure, a decarbonation reaction is in equilibrium at some temperature that is lower in a mixed-volatile fluid than it is in the presence of pure CO_2. The relation between activity of CO_2 and the displaced temperature *T* is:

$$RT \ln a_{CO_2} = \Delta G^0 - RT \ln f_{CO_2}^0 - \int_1^P \Delta V_s^0 dP \tag{7}$$

where ΔG^0 is the standard Gibbs free energy of the reaction at one bar and ΔV_s^0 is the net volume difference between the solid products and reactants. ΔG^0 is determined from the *P-T* curve of the equilibrium in pure CO_2 by setting a_{CO_2} equal to unity. Greenwood (1967) bracketed the WQC reaction (reaction A) at 1 and 2 kbar at several fluid compositions ranging from X_{CO_2}= 0.01 to 1.0 in hot-seal (Morey-type) bombs in the presence of large quantities of fluid. The fluids were not oxygen-buffered. He concluded from his results that the mixtures were nearly ideal solutions in the *P-T* range of his experiments. Additional experiments on WQC in CO_2-H_2O fluids were made by Ziegenbein and Johannes (1974, 1982) at 2, 4, and 6 kbar, using small volumes of fluid from water and silver oxalate ($Ag_2C_2O_4$) as a CO_2 source in sealed platinum capsules with either calcite and quartz or wollastonite. The capsules were buffered at relatively high oxygen fugacity (Ni-NiO) against hydrogen infiltration: Ziegenbein and Johannes (1974) estimated that there may have been as much as 5% of CH_4 plus CO in their fluid phase. From the measured temperature displacement of the equilibrium as a function of fluid composition, they inferred substantial asymmetric positive deviations from ideal mixing, with greatest deviations in the low-CO_2 range of compositions and at higher pressures, in general agreement with the volumetric measurements.

No comprehensive experimental data on the activity-composition relations in the binary are available at pressures above 6 kbar. Simple system decarbonation equilibria in the presence of H_2O-CO_2 mixtures are suitable monitors of CO_2 activity in the higher pressure range, extending the method of Greenwood (1967) and Ziegenbein and Johannes (1982). The simple dehydration reaction:

$$\underset{\text{talc}}{Mg_3Si_4O_{10}(OH)_2} = 3\ \underset{\text{enstatite}}{MgSiO_3} + \underset{\text{quartz}}{SiO_2} + H_2O \quad \text{(C) (TEQ)}$$

proved to be reversible over a wide range of CO_2-H_2O fluid compositions at high pressures, and hence a useful monitor of H_2O activity. All three equilibria, WQC, FEM, and TEQ, have *P-T* curves in the end-member systems that are reversible over large *P-T* ranges of interest to petrology. Measured thermodynamic data of high quality (heat capacities, volumes, etc.) exist for all of the solid phases involved in the reactions, and the major self-consistent data sets (Berman 1988; Mäder and Berman 1991; Berman and Aranovich 1996; Holland and Powell 1990, 1994) yield equilibrium *P-T* curves that satisfy most of the previously available experimental data. The present study capitalizes on these favorable circumstances by investigating the *P-T-*X_{CO_2} stability relations of the WQC, FEM, and TEQ reactions over extended *P-T* ranges, to determine accurate activity-concentration relations of CO_2-H_2O mixtures.

Experimental methods

Experiments were carried out in the 1.92 cm (3/4 inch) diameter piston-cylinder apparatus with the NaCl pressure medium and graphite heater sleeve. Sample geometry was identical to that described by Koziol and Newton (1995). Pressures are believed accurate to ±300 bars. In the highest temperature experiments, the pressure assembly consisted of Na-Ca glass (Kimble R-6) inner parts with an outer sleeve of NaCl. A pedestal of BN prevented the capsule from sinking through the molten glass. The glass-NaCl assemblies were similar to those used by Haselton et al. (1978). Matched W-3% Re vs. W-25% Re thermocouples were in virtual contact with the noble metal sample capsules in both types of assembly. Sample temperatures are believed accurate to ±3 °C.

The brucite to periclase + H_2O reaction and the melting point of NaCl were used in pressure calibration of the NaCl-soft glass assemblies. The former reaction was determined precisely by Aranovich and Newton (1996) to 15 kbar in the NaCl pressure cell. Welded platium capsules containing weighed amounts of synthetic brucite, synthetic periclase, and H_2O were packed tightly in finely ground glass powder at the sample site of the assembly. The pressure was raised to a nominal (gauge) pressure of 5 kbar, which was below the crushing strength of the assembly. This initial locking pressure prevented capsule blowout from H_2O expansion in heating. The temperature was then raised to 600 °C to soften the glass over much of the assembly. The assembly was next pressed to a nominal 10 kbar and held there as the sample was heated to 800-850 °C, the expected range of brucite dehydration at 10 kbar. Gauge pressure commenced to fall from glass relaxation and had to be restored continually over periods of many hours, indicating that piston-out conditions were not achieved by thermal expansion of the assemblies. A reversed bracket of 818 ± 3 °C at a nominal 10 kbar was obtained. Compared to the bracket in the frictionless assembly of 837 ± 3 °C of Aranovich and Newton (1996), the calibration gives a friction correction of the soft glass-NaCl assembly of nearly –10% at 820 °C.

Further heating of the soft glass-NaCl assemblies at pressures near 10 kbar caused the gauge pressure to increase from thermal expansion starting at about 950 °C, indicating the onset of piston-out conditions. Enough of the assembly is sufficiently soft at that sample temperature so that the large thermal expansion of the NaCl sleeve becomes a controlling factor. The melting temperature of reagent grade NaCl was determined at a nominal 10 kbar as a higher-temperature pressure calibrant. The finely ground salt was dried several hours at 320 °C, mixed intimately with ~25 vol% of fine gold filings, and the mix tightly packed in a 3 mm diameter gold tube segment and sealed by arc-welding. The capsule size and shape exactly emulated that of a buffer capsule in our experiments. The assembly was heated and pressed in stages as described above, held at 995–1020 °C for 2–3 hours, and then quenched. In experiments at 998 and 1003 °C, the salt had not melted, as evidenced by the presence of gold filings uniformly throughout the charge and by a coarse granular texture of the salt. At 1007, 1012, and 1020 °C, the gold filings had settled well toward the bottom of the capsules, and elongate clear salt crystals traversed the charge, indicative of having crystallized from a melt. The melting temperature of NaCl given by the definitive studies of Clark (1959) and Akella et al. (1969) at 10 kbar is 1004 °C. On the basis of our calibration experiments, we conclude that the soft glass-NaCl assemblies at temperature above 1000 °C are essentially frictionless.

All experiments of the present study were made with oxygen-buffered double capsules, with the exception of a few experiments on WQC above 990 °C. An initial buffer charge of about 40 mg of hematite and 4 mg of H_2O was sealed by arc-welding into a segment of 3 mm gold tubing along with the platinum sample capsule. There was rarely any detectable weight change of the buffer capsule after an experiment, and the gold capsules oozed water when punctured. The hematite was typically about 50% converted to magnetite during an experiment due to hydrogen infiltration from the NaCl pressure medium, which retained some adsorbed H_2O despite prolonged drying, and also from the hydrogen released on decomposition of oxalic acid. Experiments in the glass pressure medium showed only slight reduction of the hematite, even in experiments of several days duration at temperatures above 1000 °C. Impermeability of molten glass to hydrogen was also demonstrated by Goldsmith (1987). The gold capsules maintained their initial shape and position despite the high fluidity of the glass at experimental conditions.

Starting materials were finely ground and homogenized powder mixtures of the minerals of the WQC, FEM, and TEQ reactions, with reactant and product assemblages in about equal proportions. Most of the WQC experiments used a very pure natural wollastonite, described in Zhu et al. (1994). A synthetic wollastonite, used in some experiments, was prepared from homogenized reagent $CaCO_3$ and silica glass with pure H_2O at 860 °C and 10 kbar for 6 hours. The result was well-crystallized wollastonite with crystals of up to 0.1 mm in length whose

d-spacings were indistinguishable from those of the natural material. Talc was prepared from a mixture of synthetic enstatite, quartz, and H_2O at 10 kbar and 730 °C for 24 hours. The result was a complete yield of coarse, shiny talc having unit-cell constants (nm, deg) of $a_0 = 5.293(4)$, $b_0 = 9.163(1)$, $c_0 = 18.948(3)$, $\beta_0 = 99.38(3)$. The other materials are described in Zhu et al. (1994) and Koziol and Newton (1998).

Fluids in the experiments were generated by introducing weighed amounts of H_2O and hydrous oxalic acid, $(COOH)\cdot H_2O$, for fluids of <50 mol% CO_2, or of oxalic acid and silver oxalate ($Ag_2C_2O_4$) for more CO_2-rich fluids. The amount of volatiles in a typical charge was about 4 mg, compared to about 5 mg of solid charge. The weighing precision of the Mettler AE 240 semi-microbalance was 10^{-5} grams. Under experimental *P-T* conditions buffered at high oxygen fugacity, the oxalic acid yields a fluid of equimolar CO_2 and H_2O, and the silver oxalate yields pure CO_2. Change of the vapor composition after completion of an experiment was the major indicator of reaction progress. A retrieved platinum capsule was cleaned, frozen in liquid nitrogen and punctured with a needle while still frozen. An immediate weight loss occurred on warming, indicative of CO_2 vaporization. Subsequent drying of a capsule at 320 °C for at least 10 minutes resulted in another net weight loss, attributable to removal of the H_2O. For the TEQ experiments, the CO_2 loss could be compared with the initial CO_2 from silver oxalate and oxalic acid, because no CO_2 is absorbed in the TEQ reaction. Similarly, H_2O drying loss in the WQC and FEM experiments should match initial H_2O from water and oxalic acid. The integrity of the initial fluid composition was demonstrated by fulfillment of the above criteria, within weighing precision, in most of the experiments. Reaction progress as indicated by the weight loss measurements was verified by microscopic examination of the quenched charges and by X-ray diffraction (XRD), comparing initial and final peak heights. The latter methods were more important for the TEQ reaction, where weight changes were barely detectable because of the small amounts of H_2O absorbed or liberated in the reaction. In these experiments, most of the bracketing was accomplished in increasing temperature steps rather than by change of the vapor composition at constant temperature.

Addition of small amounts of H_2O and CO to the fluids by hydrogen infiltration conceivably could have affected the vapor-phase determination in the most CO_2-rich experiments. CO would not be distinguishable from CO_2 in the puncture weight loss, and a small amount of extra H_2O might not be detectable in the drying loss, although it could have a significant effect in lowering the decarbonation temperature of the WQC and FEM reactions in the CO_2-rich range of compositions ($X_{CO_2} > 0.8$). Thermodynamic analysis using data from Robie et al. (1978) and Shmulovich et al. (1982) shows that the combined H_2O and CO contents of an initially pure CO_2 vapor at 10 kbar and 1000 K at the equilibrium H_2 fugacity of the HM buffer would be less than 1 mol% and can be neglected. For the unbuffered WQC experiments at temperatures above 1000 °C in the soft glass assemblies, drying loss measurements were performed on a dozen quenched charges from experiments using only silver oxalate. There was no indication of an H_2O content of the final vapor. Rosenbaum and Slagel (1995) concluded from mass spectrometry of HM-buffered experiments on silver oxalate at 800 °C and 10 kbar that the vapor generated was effectively pure CO_2. For these reasons, possible contributions to our vapor phases of non-binary components was considered negliglble.

TABLE 1. Experimental data on reactions

Run no.	Duration (h)	*P* (kbar)	*T* °C	Stable phase(s)
Reaction C: Tc = 3En + Qz + H_2O				
TEQ-85	120	2	720	Tc
TEQ-113†	117	2	730	En+Qz (Ant)
TEQ-115	118	4.2	755	Tc
TEQ-116	117	4.2	765	Tc
TEQ-117	123	4.2	770	En+Qz
TEQ-227	47	6	780	Tc
TEQ-229†	72	6	785	En+Qz (Ant)
TEQ-42	117	7	780	Tc
TEQ-112	143	7	785	Tc
TEQ-45	96	7	790	En+Qz
TEQ-19	72	10	790	Tc
TEQ-111	73	10	795	Tc
TEQ-215‡	28	10	795	Tc
TEQ-16‡	70	10	800	En+Qz
TEQ-119	144	10	800	En+Qz
TEQ-255	72	14	800	Tc
TEQ-258	144	14	805	Tc
TEQ-254	72	14	810	En+Qz
Reaction A: Cc + Qz = Wol + CO_2				
WOC-76‡§	47	8	940	Cc+Qz
WOC-80‡§	70	8	946	Cc+Qz
WOC-77‡§	48	8	950	Wo
WOC-97§	47	9	992	Cc+Qz
WOC-99§	45	9	997	Wol
WOC-94§	24	10	1022	Cc+Qz
WOC-47‡§	24	10	1025	Cc+Qz
WOC-51‡§	48	10	1030	Wol
WOC-95§	26	10	1032	Wol
WOC-91§	9	12	1095	Cc+Qz
WOC-88§	7	12	1100	Wol
WOC-86§	5	14	1160	Cc+Qz
WOC-125§	4	14	1165	Wol
Reaction B: En + Mgs = Fo + CO_2				
FEM-29‡	70	10	815	En+Mgs
FEM-19‡	118	10	823	Fo

* All experiments carried out in the presence of pure H_2O or CO_2 fluid.
† Runs in which small amount of anthophyllite (Ant) was identified.
§ Runs in soft glass-NaCl setup.
‡ Runs in double capsules with HM buffer.

RESULTS OF EXPERIMENTS AND COMPARISONS

End-member reactions

It is essential to define precisely the *P-T* curves of the WQC, FEM, and TEQ reactions with pure CO_2 or H_2O vapor phases as a basis for the activity derivations. Experiments of the present study that constrain these basis equilibria are given in Table 1.

The reversed WQC bracket at a nominal 8 kbar between 946 and 950 °C may be influenced by a small amount of frictional pressure loss, since piston-out behavior was unambiguously displayed by the pressure gauge only in experiments above 950 °C. The WQC brackets are plotted in Figure 1 without frictional corrections. The unreversed wide brackets of Haselton et al. (1978) at 15 and 19 kbar appear to be consistent with the present reversals. Nearly identical brackets were secured at 10 kbar in both buffered and unbuffered experiments, which shows that the problem of hydrogen infiltration is insignificant in the soft glass pressure medium.

Tiny beads of calcite were present along cleavage planes and at margins of recrystallized wollastonites. These were undoubtedly produced in back-reaction during quenching of the glass assemblies. About 30 s were required to drop the temperature from ~1000 °C to below 100 °C in the glass assembly, compared to ~9 s in the NaCl assembly. The amount of quench calcite was much too small to have influenced determination of the reaction direction.

Figure 1 shows the predictions of the Holland and Powell (1994) and Mäder and Berman (1991) data sets. The calculated curves are in close agreement with the lower *P-T* brackets of Zhu et al. (1994) and agree with the present determinations to temperatures of at least 1020 °C. At higher temperatures and pressures, the THERMOCALC 2.3 curve is in slightly better agreement with our experiments.

Determination of the standard Gibbs free energy, ΔG^0, of the reactions from the end-member curves is based on Equation 7 with CO_2 activity set equal to unity. Three models of ΔG^0(WQC) may be erected from the data shown in Figure 1.

Model 1. The Zhu et al. (1994) brackets may be combined with the present 9 and 10 kbar brackets to produce an experimentally based model. CO_2 fugacities are taken from the tables of Shmulovich and Shmonov (1978), as was done by Zhu et al. (1994), and volumes, thermal expansion, and compressibility coefficients of the solids from Holland and Powell (1994), except for calcite. According to the measurements of Dove and Powell (1989), the volume of calcite increases rapidly as the disordering transition at 1268K (one bar) is approached. Following Zhu et al. (1994), we adopt their volume-temperature function. The derived ΔG^0 is extremely linear in the temperature range 700–1030 °C:

$$\Delta G^0(\text{WQC, exper.}) = 73938 - 140.30T,\text{K (Joules)}$$
$$r^2 = 0.99991.$$

Model 2. The Mäder and Berman (1991) data set, with their equation of state for CO_2 and simultaneously derived standard properties, yields a linear ΔG^0 in the same temperature range:

$$\Delta G^0(\text{WQC, MB}) = 75304 - 139.92T,\text{K (Joules)}$$
$$r^2 = 0.99997.$$

Model 3. The Holland and Powell (1994) THERMOCALC 2.3 data set, which incorporates the CORK equation of state of CO_2 (Holland and Powell, 1991), yields:

$$\Delta G^0(\text{WQC, HP}) = 76158 - 142.07T,\text{K (Joules)}$$
$$r^2 = 0.99990.$$

The CO_2 activities predicted by these three ΔG^0(WQC) models for calcite-quartz-wollastonite equilibrium at 6, 10, and 14 kbar and various temperatures in the present experimental range are shown in Table 2. The activities are so similar that it is almost an arbitrary choice which model to adopt at pressures to 10 kbar. For derivations at 14 kbar, there is no satisfactory way to extrapolate the tabulated CO_2 fugacities, which fact eliminates model 1 from consideration. We selected the Holland and Powell (1994) model because the CO_2 CORK equation of state is decoupled from the thermodynamic properties

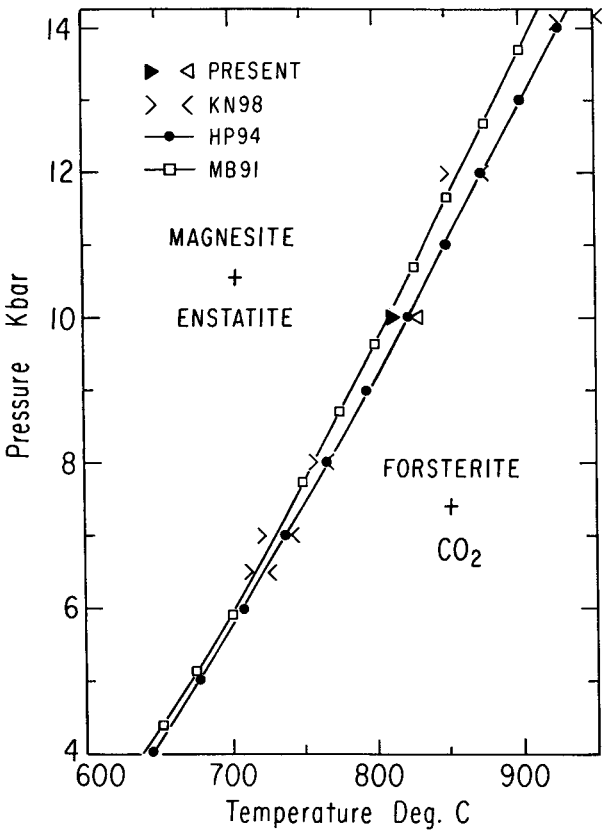

FIGURE 2. Experimental and calculated curves of the FEM reaction (Reaction B, text). The reversed brackets of Koziol and Newton (1998) and of the present study are shown. The present bracket at 10 kbar is coincident with one of Koziol and Newton (1998). The curve predicted by Holland and Powell (1994) is in slightly better agreement with the brackets than those of Mäder and Berman (1991) and is adopted for modeling CO_2 activities.

TABLE 2. CO_2 activities at experimental *P* and *T*

T, K	6 kbar			10 kbar			14 kbar	
	a_{MB}	a_{HP}	a_{EXP}	a_{MB}	a_{HP}	a_{EXP}	a_{MB}	a_{HP}
973	0.213	0.214	0.222	0.092	0.090	0.092	0.048	0.047
1023	0.340	0.337	0.335	0.145	0.144	0.145	0.077	0.076
1073	0.514	0.510	0.515	0.222	0.220	0.220	0.120	0.118
1123	0.749	0.744	0.744	0.329	0.324	0.322	0.178	0.175
1173				0.471	0.462	0.458	0.258	0.252
1223				0.658	0.641	0.634	0.362	0.351
1273				0.896	0.866	0.866	0.497	0.479
1323							0.667	0.637
1373							0.877	0.831

Notes: Values for CO_2 activities calculated for the WQC equilibrium with the three different models (text): MB = Mäder and Berman (1991); HP = Holland and Powell (1994); EXP = directly from experimental brackets using tabulated values of f_{CO_2} according to Shmulovich and Shmonov (1978).

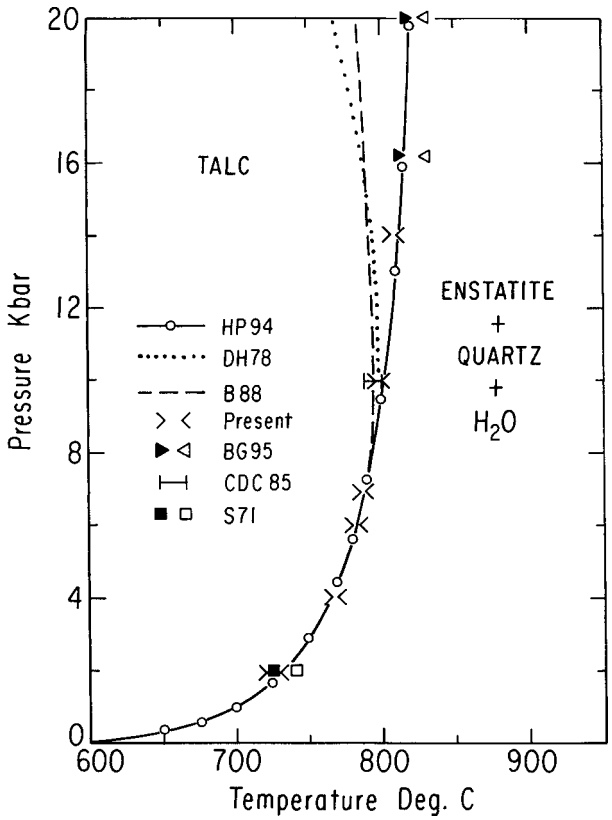

FIGURE 3. Experimental data and calculated curves of the TEQ reaction (Reaction C, text). The reversed brackets of Skippen (1971), Chernosky et al. (1985), Bose and Ganguly (1995), and the present brackets are shown. The calculated curve of Holland and Powell (1994) is in agreement with all of the brackets and is adopted as the basis for calculating H_2O activites. The curves of Berman (1988) and Delany and Helgeson (1978) assume negative d*P*-d*T* slopes above 10 kbar because of erroneously compressible H_2O equations of state.

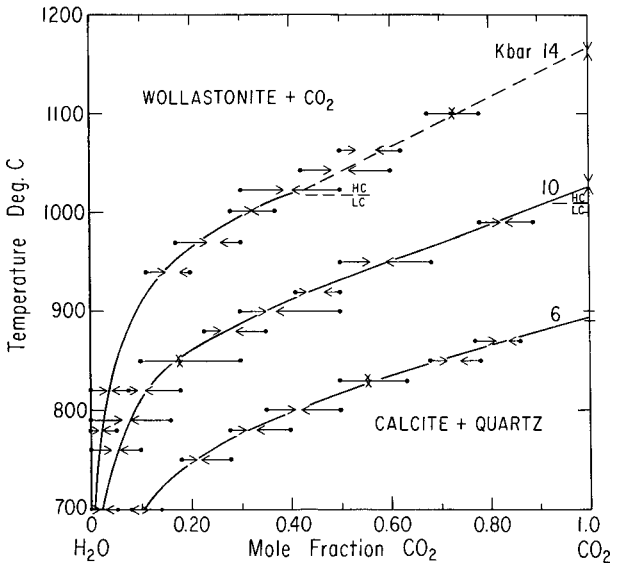

FIGURE 4. Reversed brackets on the WQC reaction with binary fluids. Plotted data are from Table 3. The arrow tails indicate the initial fluid compositions of individual experiments, and the arrowheads show the measured final fluid compositions. End-member (X_{CO_2} = 1) brackets at 10 and 14 kbar are from the present study, and the bracket at 6 kbar is based on a small extrapolation of the data of Zhu et al. (1994). The temperature of the low to high calcite transition (LC/HC) is shown at 10 and 14 kbar. Reversed brackets at 14 kbar in the interval 820–940 °C were unobtainable because of melting. The continuous curves were calculated from our best-fit model of all of the WQC, FEM, and TEQ data (Equations 9 and 10, text) with THERMOCALC 2.3. The dashed curve at 14 kbar is the approximate trend in the high calcite field, not modeled.

of the minerals, the CO_2 fugacities agree more closely with the Shmulovich and Shmonov (1978) tables, and the predicted THERMOCALC WQC curve agrees somewhat more closely with our experimental brackets than the MB curve.

The Holland and Powell (1994) and Mäder and Berman (1991) data sets also provide consistent accounts of the FEM equilibrium, as shown in Figure 2. The Holland and Powell curve satisfies all of the reversed brackets of Koziol and Newton (1998) as well as the present reversed bracket at 10 kbar (Table 1). The THERMOCALC 2.3 data set is adopted as a basis for CO_2 activity-concentration relations using the present FEM data. The corresponding ΔG^0(FEM) function may be represented closely in the range 650–960 °C by the equation:

$$\Delta G^0(\text{FEM, HP}) = 78409 - 159.31T,\text{K (Joules)}$$
$$r^2 = 0.99999.$$

Our reversals of the TEQ curve show unambiguously that it has a positive slope in the pressure range 10–15 kbar (Fig. 3), in agreement with the recent reversals of Bose and Ganguly (1995) and the deductions of Pawley and Wood (1994) based on determinations at pressures above 30 kbar with coesite rather than quartz. The curves of Delany and Helgeson (1978) and Berman (1988) assume negative d*P*/d*T* slopes above 10 kbar because of their use of equations of state of H_2O that give volumes and fugacities that are too small, as argued by Brodholt and Wood (1994). The CORK equation of state, together with the THERMOCALC 2.3 properties of the minerals, predicts a TEQ *P-T* curve that satisfies all of the reversed experimental brackets (Fig. 3) and, accordingly, is adopted in the present work. The standard Gibbs free energy of the TEQ reaction yielded by THERMOCALC 2.3 may be represented by the linear equation:

$$\Delta G^0(\text{TEQ, HP}) = 103477 - 159.25T,\text{K (Joules)}$$
$$r^2 = 0.99999.$$

Experimental data with binary H_2O-CO_2 fluids

Figure 4 shows the experimental reversals of the WQC equilibrium listed in Table 3. The opposing arrows show the measured shifts from the initial vapor compositions to the final ones. The shifts are typically large because of the large amounts of CO_2 absorbed or liberated in the reaction. The XRD patterns of the quenched charges correspondingly indicate extensive reaction. In several experiments included in Table 3, the reactions went to completion because initial fluid compositions were too far from the equilibrium ones. The small gaps between opposing arrowheads may be ascribed primarily to incomplete equili-

TABLE 3. Experimental data on the reaction Cc + Qz = Wol + CO_2 in the presence of H_2O-CO_2 fluid

Run no.	P (kbar)	T °C	Duration (h)	X_{CO_2}		Phases
				start	finish	grown
WOC-62	6	700	95	0.14	0.08	Cc+Qz
WOC-64	6	700	119	0.05	0.11	Wol
WOC-56	6	750	75	0.28	0.22	Cc+Qz
WOC-60	6	750	73	0.18	0.21	Wol
WOC-50	6	780	51	0.28	0.31	Wol
WOC-53	6	780	53	0.40	0.33	Cc+Qz
WOC-44	6	800	52	0.50	0.45	Cc+Qz
WOC-45	6	800	67	0.35	0.41	Wol
WOC-69	6	800	51	0.50	0.42	Cc+Qz
WOC-48	6	830	48	0.50	0.56	Wol
WOC-52	6	830	44	0.63	0.55	Cc+Qz
WOC-55	6	850	49	0.78	0.74	Cc+Qz
WOC-58	6	850	46	0.68	0.71	Wol
WOC-61	6	870	24	0.90	0.89	Cc+Qz
WOC-63	6	870	30	0.83	0.82	n/r
WOC-70	6	870	48	0.89	0.89	n/r
WOC-78	6	870	28	0.77	0.81	Wol
WOC-79	6	870	69	0.86	0.84	Cc+Qz
WOC-18	10	700	76	0.00	0.02	Wol
WOC-8	10	700	75	0.08	0.03	Cc+Qz
WOC-16	10	760	115	0.10	0.06	Cc+Qz
WOC-19	10	760	119	0.00	0.04	Wol
WOC-32	10	790	50	0.00	0.06	Wol
WOC-34	10	790	45	0.16	0.08	Cc+Qz
WOC-30	10	820	48	0.18	0.11	Cc+Qz
WOC-5	10	820	24	0.07	0.09	Wol
WOC-6	10	820	41	0.18	0.11	Cc+Qz
WOC-20	10	850	22	0.10	0.18	Wol
WOC-21	10	850	49	0.30	0.17	Cc+Qz
WOC-23	10	880	47	0.35	0.29	Cc+Qz
WOC-24	10	880	46	0.23	0.26	Wol
WOC-1	10	900	30	0.50	0.37	Cc+Qz
WOC-11	10	900	48	0.30	0.35	Wol
WOC-2	10	900	26	0.27	0.31	Wol
WOC-28	10	920	3	0.50	0.47	Cc+Qz
WOC-29	10	920	5	0.38	0.41	Wol
WOC-31	10	920	25	0.41	0.43	Wol
WOC-25	10	950	24	0.50	0.56	Wol
WOC-26	10	950	2	0.68	0.59	Cc+Qz
WOC-27	10	950	1	0.65	0.58	Cc+Qz
WOC-71*	10	990	23	0.89	0.83	Cc+Qz
WOC-74*	10	990	24	0.78	0.82	Wol
WOC-130	14	780	47	0.00	0.015	Wol
WOC-138	14	780	29	0.05	0.022	Cc+Qz
WOC-127	14	820	23	0.00	0.03	Wol
WOC-131	14	820	70	0.07	0.04	Cc+Qz
WOC-133	14	940	6	0.20	0.18	Cc+Qz
WOC-132	14	940	4	0.11	0.15	Cc+Qz
WOC-135	14	970	4	0.30	0.27	Cc+Qz
WOC-134	14	970	4	0.17	0.24	Wol
WOC-121	14	1000	4	0.28	0.32	Wol
WOC-129	14	1000	3	0.37	0.32	Cc+Qz
WOC-118*	14	1001	6	0.41	0.35	Cc+Qz
WOC-103*	14	1001	5	0.22	0.31	Wol
WOC-104*	14	1022	5	0.50	0.40	Cc+Qz
WOC-105*	14	1022	5	0.32	0.39	Wol
WOC-110*	14	1042	6	0.60	0.52	Cc+Qz
WOC-111*	14	1042	7	0.37	0.52	Wol
WOC-116*	14	1042	5	0.42	0.48	Wol
WOC-113*	14	1062	4	0.69	0.61	Cc+Qz
WOC-114*	14	1062	4	0.50	0.53	Wol
WOC-115*	14	1062	6	0.62	0.57	Cc+Qz
WOC-117*	14	1100	4	0.67	0.73	Wol
WOC-119*	14	1100	5	0.78	0.72	Cc+Qz

Note: (*n/r*-no clear reaction progress detected by the combination of the CO_2 weight change, optics and XRD methods).
* Runs made in soft glass-NaCl setup.

bration of the fluids with the mineral assemblages. The very small apparent overlaps of the arrowheads of a few brackets probably result from analytical error in determining the final fluid compositions. The brackets above 950 °C at 10 kbar and above 1000 °C at 14 kbar, which were determined with the soft glass-NaCl cell, appear consistent with the other brackets.

We were unable to obtain reversals of the equilibrium in a small T-X_{CO_2} range of H_2O-rich compositions at 14 kbar. Experiments at 860 and 900 °C showed complete absence of quartz in the XRD patterns, although the measured fluid compositions indicated only small reactions. This result is attributable to melting. Boettcher and Wyllie (1969) give an analysis of univariant P-T equilibria in a generalized system MO-SiO_2-H_2O, where M is a divalent metal cation and the analysis mainly models the CaO-SiO_2-H_2O system. They show melting at about 14 kbar and 900 °C, which would be analogous to the reaction:

(D) wollastonite + quartz + H_2O = liquid.

It is probable that this melting reaction occludes a small portion of the WQC curve at 14 kbar. Experiments at 820 °C with even more H_2O-rich fluids, and at 940 °C with more CO_2-rich fluids, were sharply reversible, and quartz was present in the same proportions relative to calcite, as determined by XRD peak heights, as in the starting material.

Calcite granules on recrystallized wollastonite grains were conspicuous in oil immersion mounts of charges quenched from the wollastonite + fluid field in the mid-composition range, indicating some absorption of CO_2 in the quench, with the consequent possibility of underestimation of the CO_2 content of the final fluid. Quench calcite was much more evident in experiments made with the slower-quenching soft glass-NaCl assemblies. Several experiments on oxalic acid and wollastonite were made to determine the magnitude of CO_2 absorption in quench calcite. These experiments indicate that the problem is negligible in the faster-quenching NaCl assemblies and that a possibly significant correction may be required for the soft glass-NaCl experiments at 14 kbar. Summarizing from these data, the quench-absorbed CO_2 is estimated at 1 wt% of the wollastonite present. Corresponding corrections were applied to the final fluid compositions of experiments in soft glass-NaCl assemblies where wollastonite grew. The corrections were always less than three mol% CO_2 and mostly less than 2%.

The mixed-fluid WQC data at 14 kbar seem to require some change of the dP/dT slope at temperatures above 1020 °C, the approximate location of the disordering transition at that pressure. The exact trend of the curve above 1020 °C is not determined accurately enough in the present study to define the thermodynamic properties of the high-temperature, or disordered, form of calcite.

The great effect of pressure in the range 6–14 kbar on the composition of the fluid in equilibrium with calcite, quartz, and wollastonite is evident. The increase in initial dT/dX_{CO_2} slope with pressure, from 1.5 °C per mole percent CO_2 at 6 kbar to 2.3 °C per mole percent CO_2 at 14 kbar, is a consequence of the much greater effect of pressure on the entropy of CO_2 than on the entropy of the solids, and of the orientational disorder of calcite above 1000 °C.

Reversal data on the FEM reaction are listed in Table 4 and shown in Figure 5. At 6 kbar, the equilibrium is terminated in the vicinity of 650 °C and X_{CO_2} = 0.5 by the advent of talc stability. At 10 kbar, a similar termination occurs near 700 °C and X_{CO_2} ~0.10; hence a much larger range of reversibility is ob-

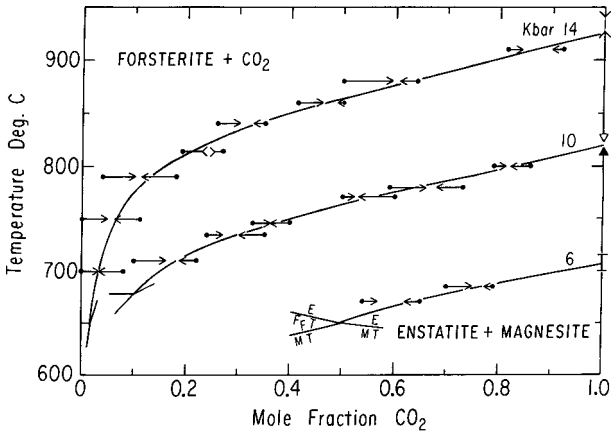

FIGURE 5. T-X_{CO_2} curves of the FEM reaction (Reaction B, text) constructed by modeling all of the present reversed WQC, FEM, and TEQ brackets with THERMOCALC 2.3. Symbols plotting reversals of the FEM reaction have the same significance as in Figure 4. The end-member bracket (X_{CO_2}= 1) at 14 kbar is from Koziol and Newton (1998), the one at 10 kbar is from the present study, and the one at 6 kbar is based on a short extrapolation of the Koziol and Newton (1998) data. The curves are terminated by invariant points produced by the onset of talc stability. Approximate positions of univariant curves at these points are shown. E = enstatite; F = forsterite; M = magnesite; T = talc.

TABLE 4. Experimental data on the reaction En + Mgs = Fo + CO_2 in the presence of H_2O-CO_2 fluid

Run no.	P (kbar)	T °C	Duration (h)	X_{CO_2} start	X_{CO_2} finish	Phases grown
FEM-36	6	670	117	0.54	0.57	Fo
FEM-40	6	670	172	0.61	0.62	n/r
FEM-42	6	670	142	0.65	0.62	En+Mgs
FEM-37	6	685	118	0.70	0.75	Fo
FEM-38	6	685	117	0.77	0.79	Fo
FEM-41	6	685	116	0.83	0.81	En+Mgs
FEM-20	10	710	118	0.22	0.19	En+Mgs
FEM-21	10	710	192	0.10	0.16	Fo
FEM-3	10	735	118	0.35	0.30	En+Mgs
FEM-5	10	735	174	0.24	0.27	Fo
FEM-7	10	746	189	0.40	0.36	En+Mgs
FEM-8	10	746	167	0.33	0.36	Fo
FEM-22	10	770	172	0.50	0.52	Fo
FEM-23	10	770	116	0.60	0.53	En+Mgs
FEM-26	10	780	168	0.59	0.66	Fo
FEM-28	10	780	168	0.73	0.68	En+Mgs
FEM-32	10	800	65	0.79	0.81	Fo
FEM-34	10	800	72	0.86	0.82	En+Mgs
FEM-65	14	700	144	0.08	0.03	En+Mgs
FEM-66	14	700	52	0.00	0.03	Fo
FEM-67	14	750	48	0.00	0.05	Fo
FEM-68	14	750	48	0.11	0.06	En+Mgs
FEM-54	14	790	118	0.18	0.11	En+Mgs
FEM-62	14	790	25	0.04	0.10	Fo
FEM-49	14	815	70	0.19	0.25	Fo
FEM-50	14	815	71	0.27	0.23	En+Mgs
FEM-48	14	840	52	0.26	0.30	Fo
FEM-51	14	840	72	0.35	0.33	En+Mgs
FEM-44	14	860	92	0.50	0.48	En+Mgs
FEM-45	14	860	48	0.39	0.44	Fo
FEM-57	14	860	48	0.41	0.46	Fo
FEM-63	14	860	6	0.50	0.49	n/r
FEM-43	14	880	72	0.50	0.59	Fo
FEM-46	14	880	48	0.64	0.61	En+Mgs
FEM-52	14	880	96	0.54	0.63	Fo
FEM-55	14	910	47	0.81	0.84	Fo
FEM-56	14	910	48	0.88	0.87	Fo
FEM-59	14	910	48	0.92	0.90	En+Mgs

Note: (*n/r*-no clear reaction progress detected by the combination of the CO_2 weight change, optics and X-ray methods).

TABLE 5. Experimental data on the reaction Tc = 3En + Qz + H_2O in the presence of H_2O-CO_2 fluid

Run no.	P (kbar)	T °C	Duration (h)	X_{CO_2} start	X_{CO_2} finish	Phases grown
TEQ-248	6	740	144	0.29	0.30	Tc
TEQ-252	6	745	125	0.29	0.29	n/r
TEQ-244	6	750	96	0.30	0.30	En+Qz
TEQ-237	6	760	118	0.31	0.30	En+Qz
TEQ-249	6	730	144	0.39	0.40	Tc
TEQ-247	6	740	258	0.40	0.40	En+Qz
TEQ-243	6	750	97	0.40	0.40	En+Qz
TEQ-225	6	725	96	0.50	0.49	Tc
TEQ-223	6	730	170	0.50	0.50	En+Qz
TEQ-238	6	710	120	0.60	0.60	En+Qz
TEQ-241	6	700	143	0.60	0.63	Tc
TEQ-239	6	690	121	0.70	0.72	En+Qz
TEQ-242	6	680	122	0.70	0.70	Tc
TEQ-250	6	675	192	0.70	0.71	Tc
TEQ-246	6	645	240	0.80	0.79	En+Qz
TEQ-251	6	635	288	0.80	0.80	Tc
TEQ-234	10	780	125	0.20	0.21	Tc
TEQ-235	10	785	167	0.21	0.20	En+Qz
TEQ-217	10	770	66	0.30	0.31	Tc
TEQ-221	10	775	70	0.30	0.30	En+Qz
TEQ-219	10	780	72	0.30	0.29	En+Qz
TEQ-230	10	760	120	0.40	0.41	Tc
TEQ-232	10	765	144	0.40	0.39	n/r
TEQ-233	10	770	163	0.40	0.39	En+Qz
TEQ-201	10	740	166	0.50	0.52	Tc
TEQ-202	10	750	188	0.50	0.49	En+Qz
TEQ-207	10	720	94	0.60	0.64	Tc
TEQ-209	10	730	144	0.60	0.61	Tc
TEQ-211	10	735	144	0.60	0.60	n/r
TEQ-203	10	740	189	0.63	0.62	En+Qz
TEQ-205	10	700	45	0.63	0.66	Tc
TEQ-208	10	705	144	0.70	0.73	Tc
TEQ-231	10	705	169	0.70	0.73	Tc
TEQ-206	10	710	96	0.70	0.70	n/r
TEQ-210	10	715	145	0.70	0.70	En+Qz
TEQ-204	10	720	118	0.70	0.70	En+Qz
TEQ-216	10	685	144	0.75	0.76	Tc
TEQ-212	10	690	121	0.78	0.78	En+Qz
TEQ-272	14	800	68	0.21	0.20	En+Qz
TEQ-273	14	792	72	0.21	0.22	n/r
TEQ-261	14	790	120	0.32	0.31	En+Qz
TEQ-263	14	785	96	0.32	0.33	Tc
TEQ-260	14	780	121	0.32	0.34	Tc
TEQ-267	14	780	93	0.40	0.40	En+Qz
TEQ-266	14	770	97	0.40	0.42	Tc
TEQ-259	14	770	95	0.50	0.48	En+Qz
TEQ-262	14	760	124	0.50	0.49	En+Qz
TEQ-264	14	755	122	0.50	0.50	n/r
TEQ-256	14	750	146	0.50	0.56	Tc
TEQ-269	14	750	169	0.60	0.57	En+Qz
TEQ-271	14	735	187	0.60	0.55	Tc+Mgs+Qz

Note: (*n/r*-no clear reaction progress detected by the combination of the H_2O weight change, optics and X-ray methods).

tainable. At 14 kbar, the FEM curve descends unimpeded in temperature across nearly the whole range of compositions. Reversibility of the FEM reaction was as sharp as for the WQC reaction. In contrast to the WQC experiments, we never observed any evidence of carbonate formation by back-reaction during the quench. The isobaric dT/dX_{CO_2} slopes of the FEM reaction are only about half as large as those of the WQC reaction, reflecting the substantially larger entropy change of the FEM reaction. Consequently, derivation of CO_2 activities from FEM are subject to greater errors than from WQC.

The TEQ data are listed in Table 5 and shown in Figure 6. Because of the small amount of H_2O absorbed or liberated in the reaction, detection of vapor composition shifts, which is the most sensitive indicator in the WQC and FEM reactions,

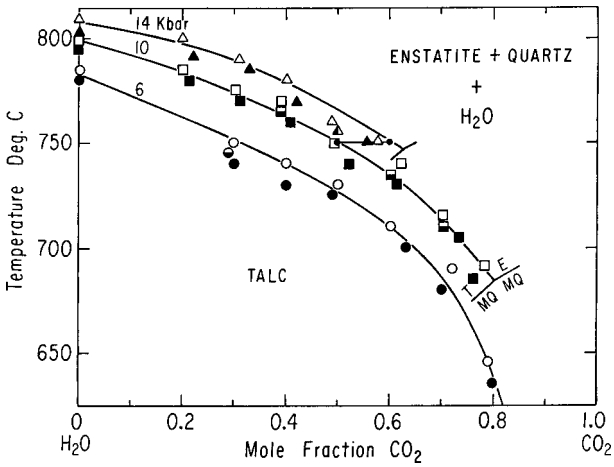

FIGURE 6. Reversed experiments of the TEQ reaction (Reaction C, text) at 6, 10, and 14 kbar. Final measured fluid compositions are plotted. The bracketing is based mainly on XRD analysis of quenched charges, rather than on shifts in fluid composition, because of the small shifts, except for the bracket at 750 °C and 14 kbar. Filled symbols indicate talc increase; open symbols indicate growth of enstatite and quartz. Half-filled symbols indicate indecisive reaction. The curves are reconstructed from our activity fit to the WQC, FEM, and TEQ data with Equations 9 and 10, text, and THERMOCALC 2.3. The curves are terminated by the onset of magnesite stability at invariant points (approximately located). T = talc; E = enstatite; M = magnesite; Q = quartz.

was not feasible. The extreme preferred orientation of enstatite needles and talc flakes in the XRD mounts created additional problems. For these reasons we were unable to produce temperature brackets tighter than 10 °C wide in the lowest temperature experiments at 6 kbar. The TEQ curve is terminated by the onset of magnesite stability at X_{CO_2} ~0.9 at 6 kbar, ~0.8 at 10 kbar, and ~0.6 at 14 kbar.

DERIVATIONS AND DISCUSSION

Theoretical predictions of mixing properties in the H_2O-CO_2 system have been mostly based on the formulation, according to simple mixing rules, of EOS parameters in the binary from the corresponding values for the pure gases (e.g., Holloway 1977; Kerrick and Jacobs 1981). The latter study remains the most widely used account of binary mixing for geological calculations and is built into the most commonly used databases (Berman 1988; Holland and Powell 1994). A similar approach was taken by Duan et al. (1992), who also introduced several adjustable parameters for mixing that had to be evaluated from the *P-V-T-X* experimental data in the binary system.

An alternative method of modeling the mixing properties was introduced in the geochemical literature by Saxena and Fei (1988) and extended by Shi and Saxena (1992). It is based on the van Laar equation for the integral excess Gibbs free energy of binary mixtures:

$$G^{ex} = X_1X_2W\{V_1^0V_2^0/[(V_1^0+V_2^0)(X_1V_1^0+X_2V_2^0)]\} \quad (8)$$

where V_1^0 and V_2^0 are the pure end-member volumes, X_1 and X_2 the mole fractions of the components ($X_1 + X_2 = 1$), and W is a regular solution energy parameter as defined by Guggenheim (1952).

For the activity coefficients, Equation 8 gives:

$$RT\ln\gamma_1 = (X_2)^2W\{V_1^0V_2^{0^2}/[(V_1^0+V_2^0)(X_1V_1^0+X_2V_2^0)^2]\} \quad (9a)$$

$$RT\ln\gamma_2 = (X_1)^2W\{V_2^0V_1^{0^2}/[(V_1^0+V_2^0)(X_1V_1^0+X_2V_2^0)^2]\} \quad (9b)$$

Applying simple intermolecular potentials from the literature, for the pair interactions H_2O-H_2O, CO_2-CO_2 and H_2O-CO_2, Saxena and Fei (1988) calculated W for the mixtures. Their model reproduces very well activity-composition relations in the binary at 500 °C and 2 kbar as measured by Shmulovich et al. (1982), and exhibits temperature and pressure dependence and sense of asymmetry of mixing similar to the MRK model of Kerrick and Jacobs (1981).

The advantage of Equations 9a and 9b is that they have very simple analytical form and are not tightly linked to any particular EOS for the end-member gases. The present analysis adopts Equations 9a and 9b for activity-composition formulations. Our approach differs, however, from that of Saxena and Fei (1988) in one important detail: instead of evaluating *W* from semi-empirical molecular physics calculations, we treated it as a fitting parameter to be determined from experiments. A simple functional form of $W(P,T)$ was chosen:

$$W = (A + BT)[1-\exp(-20P)] + CPT \quad (10)$$

with *P* in kbar and *T* in K. The "dummy" term [1–exp(–20*P*)] is inserted, following Joyce et al. (1993), to assure ideal gas behavior in the limit of low pressure; this term has a negligible effect on activity-concentration relations at pressures greater than 0.5 kbar. Volumes of CO_2 and H_2O were taken from the CORK equations of Holland and Powell (1991). All of the composition determinations of the present study were used in the fitting except for the two WQC brackets above 1040 °C at 14 kbar. This restriction is imposed by the uncertainty in ΔG^0 attending the phase change in calcite (see Fig. 1). The best-fit parameters obtained with the optimization procedure described in Aranovich and Newton (1996) are:

A = 12893 J, B = – 6.501 J/K, C = 1.0112 J/(K·kbar).

The standard deviation of the composition determinations from the best-fit equation is only 0.012 (1σ).

The mutual consistency of the three reactions is demonstrated by the fact that none of the input data show systematic deviations from the best-fit equation. If, for example, the TEQ ΔG^0 were inconsistent with the ΔG^0 of WQC or FEM, or if there were some inconsistency between the CORK predictions for H_2O and CO_2, the TEQ data should show deviations all of one sign, because the database is somewhat dominated by the decarbonation data. In fact, the deviations of all of the input data from the predicted curves appear to be distributed randomly.

Figure 7 compares the activity-concentration relations predicted by the present model with those obtained from the MRK model of Kerrick and Jacobs (1981) at 800 °C and four pressures. At 2 and 6 kbar the agreement is quite remarkable: our data are consistent with Kerrick and Jacobs (1981) within fitting uncertainty. The predicted asymmetry is almost exactly the same for both formulations despite their dissimilarities. This is probably because the disparate volumes of CO_2 and H_2O, reflected in the different **a** and **b** parameters of the MRK equation, enter the activity-concentration relations in a way analogous to the present formulation. At 10 kbar our reconstruction gives slightly

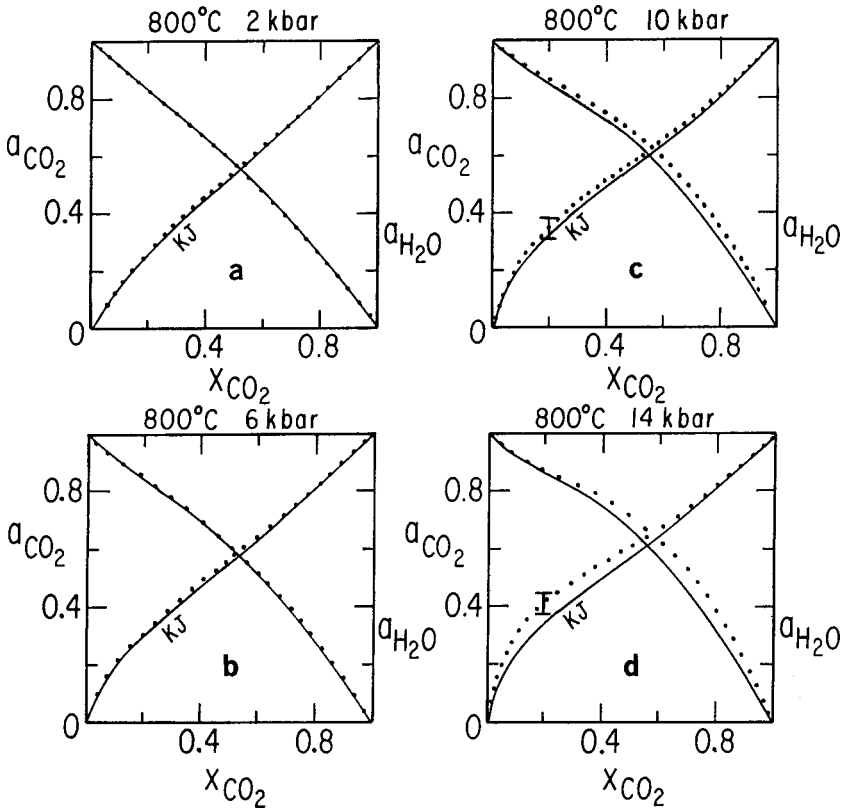

FIGURE 7. Activity-concentration relations of the system CO_2-H_2O at 800 °C and 2, 6, 10, and 14 kbar from Kerrick and Jacobs (1981: continuous curves) and those predicted by the present modeling of the WQC, FEM, and TEQ experimental brackets (dots). The standard deviation (2σ) of our CO_2 activities in the low mole fraction range is ±0.035, as shown in 7c and 7d. The differences between the two models are significant at 14 kbar.

larger deviations from ideality than the model of Kerrick and Jacobs (1981). At 14 kbar the discrepancy is more evident: our values are about what would be predicted by Kerrick and Jacobs for 30–40 kbar.

An approximate assessment of the uncertainties associated with our measurements shows that our CO_2 activities at 14 kbar are significantly different from those of Kerrick and Jacobs (1981). Sources of error include temperature and pressure control in the experiments, quality of the analyses of the quenched fluids, which depends on weighing precision, and the degree of equilibration of the charges. THERMOCALC 2.3 is accepted as an absolute standard. This assumption is justified by the fact that our activities are obtained from experimental points by free energy differences within an internally consistent data set, and do not depend strongly on the particular data set adopted, as shown in Table 2. The assumption of virtually binary fluids has been justified.

The maximum departures from ideality of the component activities occur at low mole fractions and are greatest, at a given temperature, at the highest pressures. At 800 °C, 14 kbar and $X_{CO_2} = 0.2$, Equations 9 and 10 indicate that our temperature uncertainty of 3 °C is associated with an uncertainty in a_{CO_2} of 0.0033, and our pressure uncertainty of 300 bars generates an uncertainty in a_{CO_2} of 0.0042. It is considered that our standard deviation of measured compositions from the best-fit curves accounts for combined errors from incomplete equilibration and analytical precision. The observed standard deviation of 0.012 in X_{CO_2} translates to an uncertainty of 0.0101 in a_{CO_2}, using the calculated da_{CO_2}/dX_{CO_2} of 0.843 at 800 °C, 14 kbar and $X_{CO_2} = 0.2$. A one-sigma uncertainty in a_{CO_2} associated with a compositional measurement in this parameter range may be estimated as the sum of these uncertainties, or 0.0176. The corresponding two-sigma uncertainty of 0.0352 is plotted in Figure 7d.

Based on this analysis, we conclude that our CO_2 activities at 14 kbar are significantly more non-ideal than those of Kerrick and Jacobs (1981). An uncertainty of similar magnitude may be derived for the same temperature and composition at 10 kbar. Figure 7c indicates that our a_{CO_2} values at 10 kbar are not significantly different from those of Kerrick and Jacobs (1981). Our compositional data for the TEQ reaction are not sufficiently comprehensive to perform a reliable analysis of uncertainty in a_{H_2O}; however, the Gibbs-Duhem relation requires that non-ideality in CO_2 be reflected in commensurate non-ideality in H_2O, as shown in Figure 7.

A summary conclusion is that non-ideality in CO_2-H_2O solutions increases more rapidly above 10 kbar than given by the Kerrick and Jacobs model. At 0.5 kbar and 500 °C, activities calculated with Equations 9 and 10 are appreciably higher than those predicted by Kerrick and Jacobs, and actually agree very closely with the recent measurements of Anovitz et al. (1998). The predicted activity-concentration relations of Saxena and Fei (1988) at 800 °C and 2 and 10 kbar, shown in their Figure 5, are nearly identical to those depicted in our Figure 7. We could not make a more extensive comparison because we were unable to reproduce their activity-concentration calculations using their formulas. The semi-empirical reconstruction of Duan et al. (1996) for the H_2O-CO_2 system predicts CO_2 and H_2O activities at 800 °C and 2–10 kbar very close to those of Kerrick

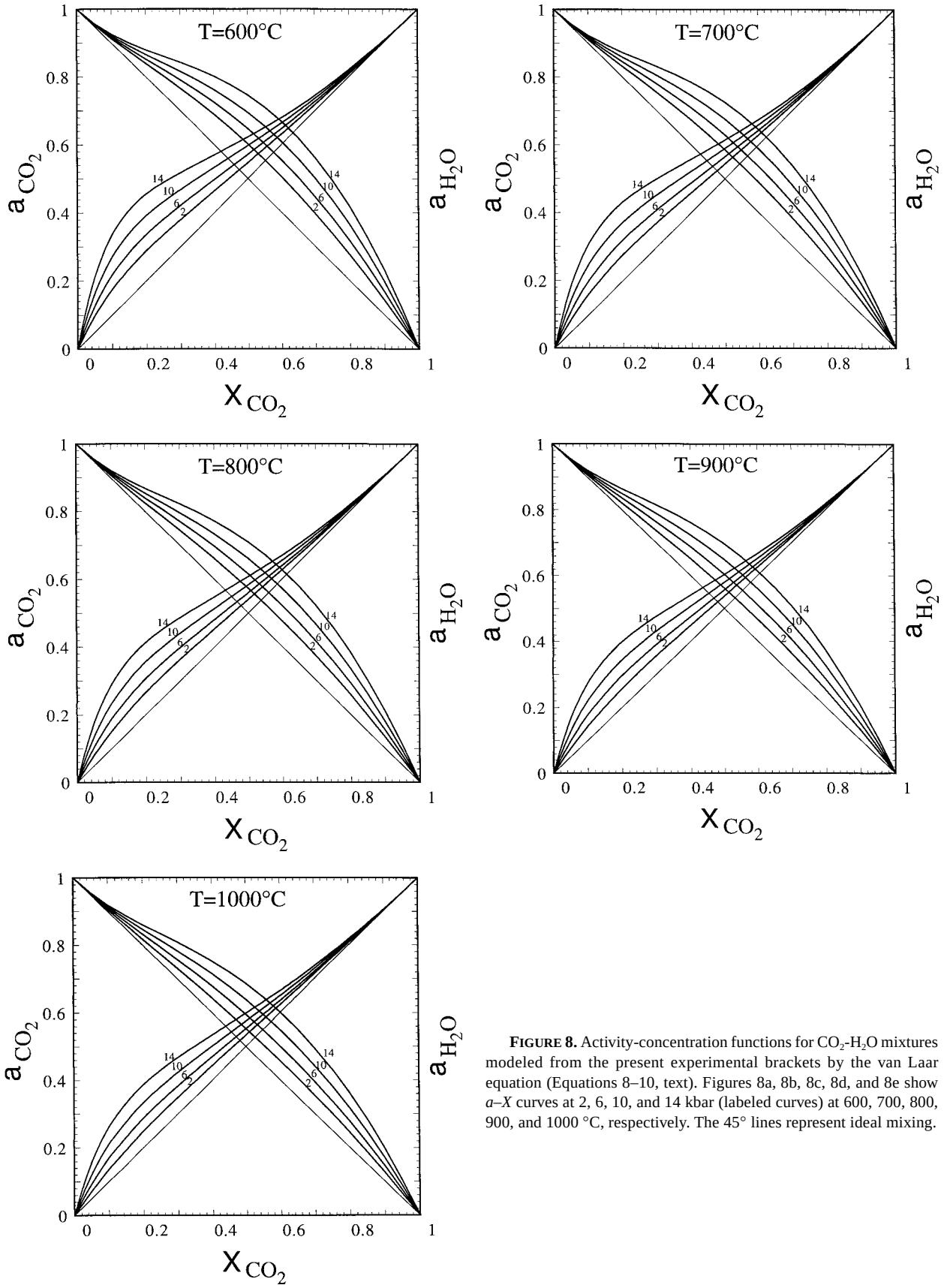

FIGURE 8. Activity-concentration functions for CO_2-H_2O mixtures modeled from the present experimental brackets by the van Laar equation (Equations 8–10, text). Figures 8a, 8b, 8c, 8d, and 8e show *a–X* curves at 2, 6, 10, and 14 kbar (labeled curves) at 600, 700, 800, 900, and 1000 °C, respectively. The 45° lines represent ideal mixing.

and Jacobs (1981). Figure 8 shows activity-concentration relations of CO_2-H_2O mixtures predicted by the present reconstruction at 600–1000 °C and 2, 6, 10, and 14 kbar.

APPLICATION TO PETROLOGY

The present formulas for CO_2 and H_2O activities in their mixtures may be used for calculations of mineralogical equilibria and fluid-rock interaction over an extended *P-T* range applicable to deep crust and upper mantle processes: 600–1100 °C and 6–14 kbar. It is likely that calculations down to one kbar or below at temperatures down to 500° C will be reasonably accurate with the present formulas. Calculations of interest include granulite facies metamorphic reactions, especially involving calc-silicate rocks, vapor phase modeling of magmatic processes, and interactions of mafic and ultramafic rocks with a dense CO_2-H_2O vapor phase, as in mantle metasomatism.

It is to be emphasized that the three binary parameters A, B, and C, may be used with equal success along with any reasonably accurate EOS of CO_2 and H_2O, and are not tied to the THERMOCALC 2.3 data set or the CORK EOS. For example, at 800 °C and 10 kbar the difference between CO_2 molar volumes from CORK (36.18 cm^3) and the tables of Shmulovich and Shmonov (1978) (34.97 cm^3) is ~4%. Yet the activities calculated with Equation 9 differ by no more than 2–3 thousandths for both CO_2 and H_2O in the entire compositional range, which is quite negligible for most purposes.

Solutions with the additional component NaCl at elevated pressures will have dramatically higher a_{CO_2} and decreased a_{H_2O}, leading to immiscibility of the two volatiles, even for only moderate NaCl concentrations, as shown by the calculations of Bowers and Helgeson (1983) and Duan et al. (1995). Chlorine is likely to be available in metamorphism of metasediments, ore-forming processes involving vapor transport, and gases of magmatic origin. Calculations at pressures greater than those addressed by the earlier workers are desirable, and the present work provides a baseline that, along with the experimental work on the H_2O-NaCl and H_2O-KCl binaries (Aranovich and Newton 1996, 1997), may be useful in further experimental and theoretical definition of complex natural deep-seated fluids.

ACKNOWLEDGMENTS

This work was supported by a National Science Foundation grant to the authors, no. EAR-9632591. Information and counseling about the THERMOCALC program was provided by Tim Holland. We also thank Zhenhao Duan for providing the results of *a-X* calculations according to Duan et al. (1996). The critical comments of Bernie Wood, Terry Gordon, and Jim Blencoe on an earlier version of this paper resulted in considerable improvement.

REFERENCES CITED

Akella, J., Vaidya, S.N., and Kennedy, G.C. (1969) Melting of sodium chloride at pressures to 65 kbar. The Physical Review, 185, 1135–1140.

Anovitz, L.M., Blencoe, J.G., Joyce, D.B., and Horita, J. (1998) Precise measurement of the activity/composition relations of H_2O-N_2 and H_2O-CO_2 fluids at 500 °C, 500 bars. Geochimica et Cosmochimica Acta, 62, 815–829.

Aranovich, L.Y. and Newton, R.C. (1996) H_2O activity in concentrated NaCl solutions at high pressures and temperatures measured by the brucite-periclase equilibrium. Contributions to Mineralogy and Petrology, 125, 200–212.

——(1997) H_2O activity in concentrated KCl and KCl-H_2O solutions at high temperatures and pressures measured by the brucite-periclase equilibrium. Contributions to Mineralogy and Petrology, 127, 261–271.

Berman, R.G. (1988) Internally-consistent thermodynamic data for minerals in the system Na_2O-K_2O-CaO-MgO-FeO-Fe_2O_3-Al_2O_3-SiO_2-TiO_2-H_2O-CO_2. Journal of Petrology, 29, 445–522.

Berman, R.G. and Aranovich, L.Ya. (1996) Optimized standard state and solution properties of minerals: I. Model calibration for olivine, orthopyroxene, cordierite, garnet, and ilmenite in the system FeO-MgO-CaO-Al_2O_3-SiO_2-TiO_2. Contributions to Mineralogy and Petrology, 126, 1–24.

Boettcher, A.L. and Wyllie, P.J. (1969) The system CaO-SiO_2-CO_2-H_2O: III. Second critical end-point on the melting curve. Geochimica et Cosmochimica Acta, 33, 611–632.

Bose, K. and Ganguly, J. (1995) Experimental and theoretical studies of the stabilities of talc, antigorite and phase A at high pressures with applications to subduction processes. Earth and Planetary Science Letters, 136, 109–121.

Bottinga, Y. and Richet, P. (1981) High pressure and temperature equation of state and calculation of the thermodynamic properties of gaseous carbon dioxide. American Journal of Science, 281, 615–660.

Bowers, T.S. and Helgeson, H.C. (1983) Calculation of the thermodynamic and geochemical consequences of nonideal mixing in the system H_2O-CO_2-NaCl on phase relations in geologic systems: Equation of state for H_2O-CO_2-NaCl fluids at high pressures and temperatures. Geochimica et Cosmochimica Acta, 47, 1247–1275.

Brodholt, J.P. and Wood, B.J. (1994) Measurements of the PVT properties of water to 25 kbars and 1600 °C from synthetic fluid inclusions in corundum. Geochimica et Cosmochimica Acta, 58, 1083–1104.

Bulakh, A.G. (1979) Thermodynamic properties and phase transitions of water up to 1000 °C and 100 kbar. International Geology Review, 21, 92–103.

Burnham, C.W., Holloway, J.R., and Davis, N.F. (1969) Thermodynamic properties of water to 1,000 °C and 10,000 bars. Geological Society of America Special Paper 132, 1–96.

Chernosky, J.V. Jr., Day, H.W., and Caruso, L.L. (1985) Equilibria in the system MgO-SiO_2-H_2O: I. Experimental determination of the stability of Mg-anthophyllite. American Mineralogist, 70, 223–236.

Chou, I.M. and Williams, R.J. (1979) The activity of H_2O in super-critical fluids: H_2O-CO_2 at 600 °C and 700 °C at elevated pressures. Lunar and Planetary Science Conference Proceedings, 10, 201–203.

Clark, S.P. Jr. (1959) Effect of pressure on the melting point of eight alkali halides. Journal of Chemical Physics, 31, 1526–1531.

Delany, J.M. and Helgeson, H.C. (1978) Calculation of the thermodynamic consequences of dehydration in subducting oceanic crust to 100 kb and <800 °C. American Journal of Science, 278, 638–686.

Dove, M.T. and Powell, B.M. (1989) Neutron diffraction study of the tricritical orientational order-disorder phase transition in calcite at 1260 K. Physics and Chemistry of Minerals, 16, 503–507.

Duan, Z., Moeller, N., and Weare, J.H. (1992) An equation of state for the CH_4-CO_2–H_2O-system: II. Mixtures from 50 to 1000 °C and 0 to 1000 bar. Geochimica et Cosmochimica Acta, 56, 2619–2631.

——(1995) Equation of state for the NaCl-H_2O-CO_2 system: Prediction of phase equilibria and volumetric properties. Geochimica et Cosmochimica Acta, 59, 2869–2882.

——(1996) A general equation of state for supercritical fluid mixtures and molecular dynamics simulation of mixture *P-V-T-X* properties. Geochimica et Cosmochimica Acta, 60, 1209–1216.

Frost, D.J. and Wood, B.J. (1995) Experimental determination of the graphite-C-O equilibrium and CO_2 fugacities at high temperature and pressure. Contributions to Mineralogy, 121, 303–308.

——(1997a) Experimental determination of the fugacity of CO_2 and graphite/diamond stability from 35 to 77 kbar at 925 to 1650 °C. Geochimica et Cosmochimica Acta, 61, 1565–1574.

——(1997b) Experimental measurements of the properties of H_2O-CO_2 mixtures at high pressures and temperatures. Geochimica et Cosmochimica Acta, 61, 3301–3309.

Goldsmith, J.R. (1987) Al/Si interdiffusion in albite: effect of pressure and the role of hydrogen. Contributions to Mineralogy and Petrology, 95, 311–321.

Greenwood, H.J. (1967) Wollastonite: stability in H_2O-CO_2 mixtures and occurrence in a contact-metamorphic aureole near Salmo, British Columbia, Canada. American Mineralogist, 52, 1669–1680.

——(1969) The compressibility of gaseous mixtures of carbon dioxide and water between 0 and 500 bars and 450° and 800° centigrade. American Journal of Science, 267-A, 191–208.

——(1973) Thermodynamic properties of gaseous mixtures of H_2O and CO_2 between 450° and 800 °C and 0 to 500 bars. American Journal of Science, 273, 561–571.

Guggenheim, E.A. (1952) Mixtures, 365 p. Clarendon Press, Oxford.

Haar, C., Gallagher, J.S., and Kell, G.S. (1984) NBS/NRC Steam Tables, 400 p., Hemisphere, Washington D.C.

Halbach, H., and Chatterjee, N.D. (1982) An empirical Redlich-Kwong-type equation of state for water to 1000 °C and 200 kbar. Contributions to Mineralogy and Petrology, 79, 337–345.

Haselton, H.T. Jr., Sharp, W.E., and Newton, R.C. (1978) CO_2 fugacity at high temperatures and pressures from experimental decarbonation reactions. Geophysical Research Letters, 5, 753–756.

Holland, T.J.B. and Powell, R. (1990) An enlarged and updated internally consistent thermodynamic data set with uncertainties and correlations: the system K_2O-

Na_2O-CaO-MgO-MnO-FeO-Fe_2O_3-Al_2O_3-TiO_2-SiO_2-C-H_2-O_2. Journal of Metamorphic Geology, 8, 89–124.

——(1991) A Compensated Redlich-Kwong equation for volumes and fugacities of CO_2 and H_2O in the range 1 bar to 50 kbar and 100–1600 °C. Contributions to Mineralogy and Petrology, 109, 265–273.

——(1994) THERMOCALC, version 2.3 (computer program with thermodynamic data set).

Holloway, J.R. (1977) Fugacity and activity of molecular species in supercritical fluids. In D. G. Fraser, Ed., Thermodynamics in geology, 161–181 p., Reidel, Dordrecht. Joyce, D.B., Blencoe, J.G., and Burch, T.E. (1993) A two-parameter Margules method for modeling the thermodynamic mixing properties of H_2O-CO_2 fluids. Geological Society of America, Abstracts with Programs, 25, p.A–212.

Joyce, D.B. and Holloway J.R. (1993) An experimental determination of the thermodynamic properties of H_2O-CO_2-NaCl fluids at high pressures and temperatures. Geochimica et Cosmochimica Acta, 57, 733–746.

Kerrick, D.M. and Jacobs, G.K. (1981) A modified Redlich-Kwong equation for H_2O, CO_2 and H_2O-CO_2 mixtures at elevated pressures and temperatures. American Journal of Science, 281, 735–767.

Koziol, A.M. and Newton, R.C. (1995) Experimental determination of the reactions magnesite + quartz = enstatite + CO_2 and magnesite = periclase + CO_2 and enthalpies of formation of enstatite and magnesite. American Mineralogist, 80, 1252–1260.

——(1998) Experimental determination of the reaction: Magnesite + enstatite = forsterite + CO_2 in the ranges 6–25 kbar and 700–1100 °C. American Mineralogist, 83, 213–219.

Mäder, U.K. and Berman, R.G. (1991) An equation of state for carbon dioxide to high pressure and temperature. American Mineralogist, 76, 1547–1559.

Newton, R.C. and Sharp, W.E. (1975) Stability of forsterite + CO_2 and its bearing on the role of CO_2 in the mantle. Earth and Planetary Science Letters, 26, 239–244.

Pawley, A.R. and Wood, B.J. (1994) Talc dehydration to 50 kbar: Constraints on the volume of H_2O at high pressure. Mineralogical Magazine, 58-A, 698–699.

Redfern, S.A.T., Salje, E., and Navrotsky, A. (1989) High temperature enthalpy at the orientational order-disorder transition in calcite: implications for the calcite/aragonite phase equilibrium. Contributions to Mineralogy and Petrology, 101, 479–484.

Robie, R.A., Hemingway, B.S., and Fisher, J.R. (1978) Thermodynamic properties of minerals and related substances at 298.15 K and 1 bar (10^5 pascals) pressure and at higher temperatures. U. S. Geological Survey Bulletin, 1452, 1–456.

Rosenbaum, J.M. and Slagel, M.M. (1995) C-O-H speciation in piston-cylinder experiments. American Mineralogist, 80, 109–114.

Saxena, S.K. and Fei, Y. (1988) Fluid mixtures in the C-H-O system at high pressure and temperature. Geochimica et Cosmochimica Acta, 52, 505–512.

Seitz, J.C. and Blencoe, J.G. (1996) Experimentally determined volumetric properties of CO_2-H_2O mixtures at 400 °C and pressures up to 1000 bars. Geological Society of America Abstracts with Programs, 28, A–159.

Sharp, W.E. (1962) The thermodynamic functions for water in the range 10 to 1000 °C and 1 to 250,000 bars. University of California, E. O. Lawrence Radiation Laboratory Publication UCRL-718 (Chemistry UC-4), 1–50.

Shi, P. and Saxena, S.K. (1992) Thermodynamic modeling of the C-H-O-S fluid system. American Mineralogist, 77, 1038–1049.

Shmonov, V.M. and Shmulovich, K.I. (1974) Molar volumes and equation of state of CO_2 at temperatures from 100–1000 °C and pressures from 2000–10000 bars. Doklady Akademiia Nauk SSSR, 217, 935–938.

Shmulovich, K.I. (1988) Carbon dioxide in high-temperature processes of mineral formation, 232 p., Nauka Press, Moscow (in Russian).

Shmulovich, K.I. and Shmonov, V.M. (1978) Tables of thermodynamic properties of gases and liquids, Volume 3: Carbon dioxide, 167 p. USSR Academy of Sciences, Bureau of Standards, Moscow. Shmulovich, K.I., Shmonov, V.M., and Zharikov, V.A. (1982) The thermodynamics of supercritical fluid systems. In S.K. Saxena, Ed., Advances in physical geochemistry, Volume 3, p. 173–190, Springer, New York.

Skippen, G.B. (1971) Experimental data for reactions in siliceous marbles. Journal of Geology, 79, 451–481.

Sterner, S.M. and Bodnar, R.J. (1991) Synthetic fluid inclusions X: Experimental determination of P-V-T-X properties in the CO_2-H_2O system to 6 kbar and 700 °C. American Journal of Science, 291, 1–54.

Zhu, H., Newton, R.C., and Kleppa, O.J. (1994) Enthalpy of formation of wollastonite ($CaSiO_3$) and anorthite ($CaAl_2Si_2O_8$) by experimental phase equilibrium measurements and high-temperature solution calorimetry. American Mineralogist, 79, 134–144.

Ziegenbein, D., and Johannes, W. (1974) Wollastonitbildung aus Quarz und Calcit. Fortschritte der Mineralogie, 52, 77–79.

——(1982) Activities of CO_2 in supercritical CO_2-H_2O mixtures, derived from high-pressure mineral equilibrium data. In W. Schreyer, Ed., High-pressure researches in geoscience, p. 493–500, Schweitzerbart'sche Verlagsbuchhandlung, Stuttgart.

MANUSCRIPT RECEIVED MAY 27, 1998
MANUSCRIPT ACCEPTED APRIL 23, 1999
PAPER HANDLED BY JAMES G. BLENCOE